FULL-SCALE TEST STUDY OF BEARING BEHAVIOUR OF LARGE DIAMETER SUPER-LONG STEEL PIPE PILES IN OFFSHORE WIND FARM

Jiang Xu[1 *], Yuhe Xia[1], Weiming Gong[2], Huifang Deng[3], Zhengwei Bai[3], Yuanbing Chen[4]

1.*College of Architecture Science Engineering Yangzhou University, Yangzhou, China;*
2. *School of Civil Engineering, Southeast University, Nanjing, China*
3. *Nuclear industry Huzhou Survey, Planning and Design Institute Co., Ltd, Huzhou, China;*
4.*Yangzhou Water Conservancy Construction Engineering Co., Ltd, Yangzhou, China.*

https://doi.org/10.56295/AGJ6032

ABSTRACT

Steel pipe piles have been widely used in offshore wind farms, offshore platforms, and other offshore engineering. Due to difficulties of the offshore field test, the full-scale field test data of the large diameter super-long steel pipe pile are still very limited. Based on the East China Sea Bridge Wind Farm project, the axial and lateral bearing capacity test were carried out on four super-long steel pipe piles, two of which are vertical piles and two are inclined piles. Through the test and analysing, the axial and lateral ultimate bearing capacity of the piles was determined, and the axial ultimate bearing capacity of inclined piles was significantly smaller than that of vertical piles. Furthermore, based on the test results and the measured strain data, the equivalent conversion results, the distributions of axial force and shaft resistance, the relationship between the shaft resistance and relative displacement of pile-soil interface, the pile shaft deflection, and the *p-y* curves in different soil layers were also discussed. Finally, the conclusions are presented, and it can provide a reference for designing the super-long steel pipe piles in offshore engineering.

1 INTRODUCTION

Increasing energy demand and pressure on environmental protection have put the development and use of green energy at the forefront. Apart from nuclear energy, which now generates 6.5% of world's energy, renewable energy such as solar, geothermal, water, wind, and biomass is steadily increasing, now generating up to 13.1% of global energy consumption (IEA, 2007). Over the last 10 years, offshore wind farms have grown rapidly, becoming a new field of development in the wind power industry(Snyder and Kaiser 2009; Haiderali and Madabhushi 2012; Liu et al. 2015). The 13th Five-year Plan for Wind Power Development promulgated by China's National Energy Administration mentioned that by the end of 2020, the cumulative installed wind power capacity would reach to 210 million kilowatts and wind power will generate 420 billion kilowatt-hours per year.

Since steel pipe piles have lots of advantages, such as strong bearing capacity, good performance of penetration soil, making simple, easy construction, therefore, they are widely used in offshore wind farms, offshore platforms, and another offshore engineering. As increasing demand for large diameter pipe piles in offshore engineering, considerable effort has been made in recent years to investigate the loading behaviour and bearing capacity of pipe piles (Paikowsky and Whitman 1990; Jardine 1996; De Nicola and Randolph 1997; Nicola and Randolph 1999; Lehane and Gavin 2001; Paik and Salgado 2003; Fan and Long 2005; Yu and Yang 2011; Liu et al. 2015; Feng, Lu, and Shi 2016; Li et al. 2016), leading to improved understanding and design methods. The foundations of the wind turbine are subjected to a large axial load, overturning moments, waves and lateral loads (Alari and Raudsepp 2012), therefore, higher requirements were needed for the bearing capacity and deformation of the wind foundation. To achieve the large bearing capacity and reduce deformation, long or super-long piles with larger diameters piles are required to penetrate the deep soil layers. Now, the specified definition of a super-long pile remains unclear (Zou and Zhao 2013; Li et al. 2016) but often refers to a pile over 50 m long or with a length-to-diameter ratio that exceeds 100. For the super-long piles, the performance and behaviour of this type of pile are different from those of traditional small-scale piles. Thus, the traditional calculation methods and load transfer mechanism obtained from research on small-scale piles are maybe also not suitable for super-long piles. Although, many studies have been conducted to clarify these issues (Feng et al. 2004; Lesny and Wiemann 2006; Gao, Zeng, and Zhu 2011; Wang, Li, and Wu 2011; Wang et al. 2012; Zou and Zhao 2013; Li et al. 2016) , but, many research on super-long piles has primarily focused on case-in-place bored piles, thus, the documents and existing literature on super-long steel pipe piles are sparse. Moreover, due to difficulties of the offshore field test, the laboratory tests or in-situ tests of small piles were usually carried out to speculate and analysis the bearing capacity of large diameter steel pipe piles used for offshore wind turbine foundation, therefore, the literature of full-scale field test data of the large diameter super-long steel pipe pile is still very limited, and it is necessary and meaningful to research on the bearing behavior of large diameter super-long steel pipe piles by full-scale filed tests.

In this study, based on the East China Sea Bridge Wind Farm project, four full-scale piles tests of axial bearing capacity test and lateral bearing capacity were conducted. According to the test data, it got the axial ultimate bearing capacity of the vertical piles and inclined piles and lateral bearing capacity of the vertical piles, the distributions of axial force and shaft resistance, and the relationship between the shaft resistance and relative displacement of different soil layers. Moreover, based on the lateral test results, the results of the bending moment of pile shaft, the pile shaft deflection, and the *p-y* curves in different soil layers of 40#ZZ1 was also obtained. Finally, some conclusions and the data from this study are also valuable for the design and evaluation of current applications of super-long steel pipe piles.

2 BACKGROUND

The second phase project of the East China Sea Bridge offshore wind farm located in the west side of the East China Sea Bridge of Shanghai city (Figure 1). The seabed topography in the project site is generally flat, the seabed beach surface elevation is -10.94 to -11.06m, and the average sea level elevation is 0.34m. The tides in the tested area were mainly affected by the forward tidal waves in the East China Sea, which was an informal half-day shallow water tide. According to the extreme high and low water level of Luchao port for many years, it was found that the high tide level and the low tide level were 2.54m and -1.76m respectively.

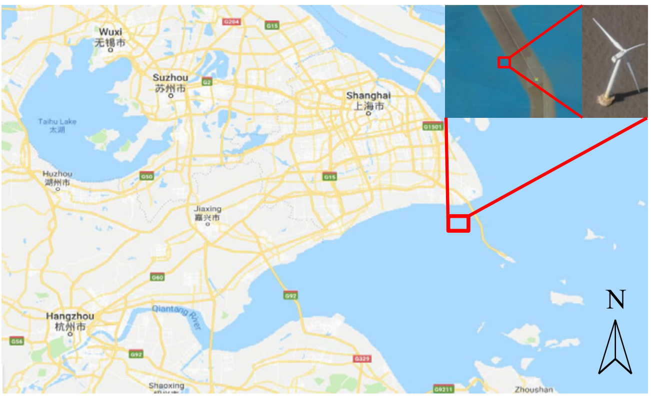

Figure 1: The location of the project in Shanghai city, China

There are 28 wind turbines arranged in five rows in the wind farm, and each turbine foundation concluded a vertical pile (D=1700mm) and eight inclined piles (D=1700mm, the slope is 5.5: 1 and inclination is 12°). These eight inclined piles are uniformly arranged on the circumference, the centre of the circumference is also the centre of concrete foundation cap, and the radius is 5.00m, and the layout of the 40# (41#) test platform is shown in Figure 2. The material of steel pipe pile is Q345C, and the wall thickness of the pile is not uniform, the thickness of the upper segment is 30mm and the lower segment was 25mm (Figure 3). The elevation of the test piles and steel gauges, geological conditions of the test pile, and parameters of the test piles are shown in Figure 3 and Table 1. Furthermore, by carrying out indoor geotechnical tests such as moisture content test, liquid limit and plastic limit combined determination test and direct shear test, the soil parameters such as density (ρ), moisture content (w), liquid limit (w_L), plastic limit (w_P), cohesion (c) and internal friction angle (φ) et.al were measured, the results as shown in Table 2.

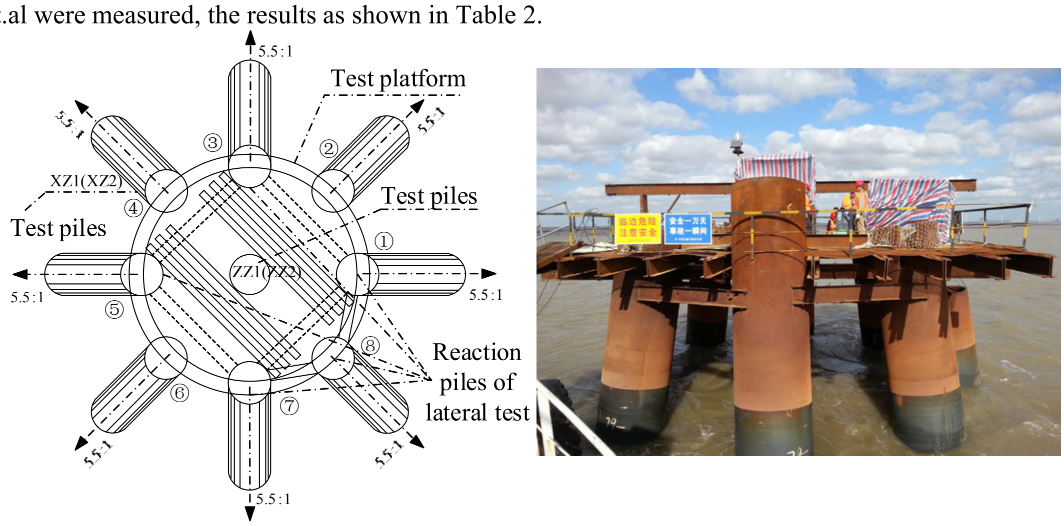

Figure 2: The layout of the 40#(41#) test platform

Table 1: Parameters of test piles

Test pile	40#ZZ1	40#XZ1	41#ZZ2	41#XZ2
Type of pile	Vertical pile	Inclined pile	Vertical pile	Inclined pile
Diameters (mm)	1700	1700	1700	1700
Elevation of pile head (m)	+5.2	+4.4	+5.2	+4.4
Elevation of pile base (m)	-80.00	-80.11	-80.00	-80.11
Design lengths(m)	85.20	85.90	85.20	85.90
Thickness of the pipe piles	30/25 mm	30/25mm	30/25mm	30/25mm
Design axial load of test (kN)	38000	27000	38000	27000
Design lateral load of test (kN)	480	—	480	—
Elevation of load cell (m)	-78.00	-78.11	-78.00	-78.11
Elevation of mud surface (m)	-11.00	-11.00	-11.00	-11.00

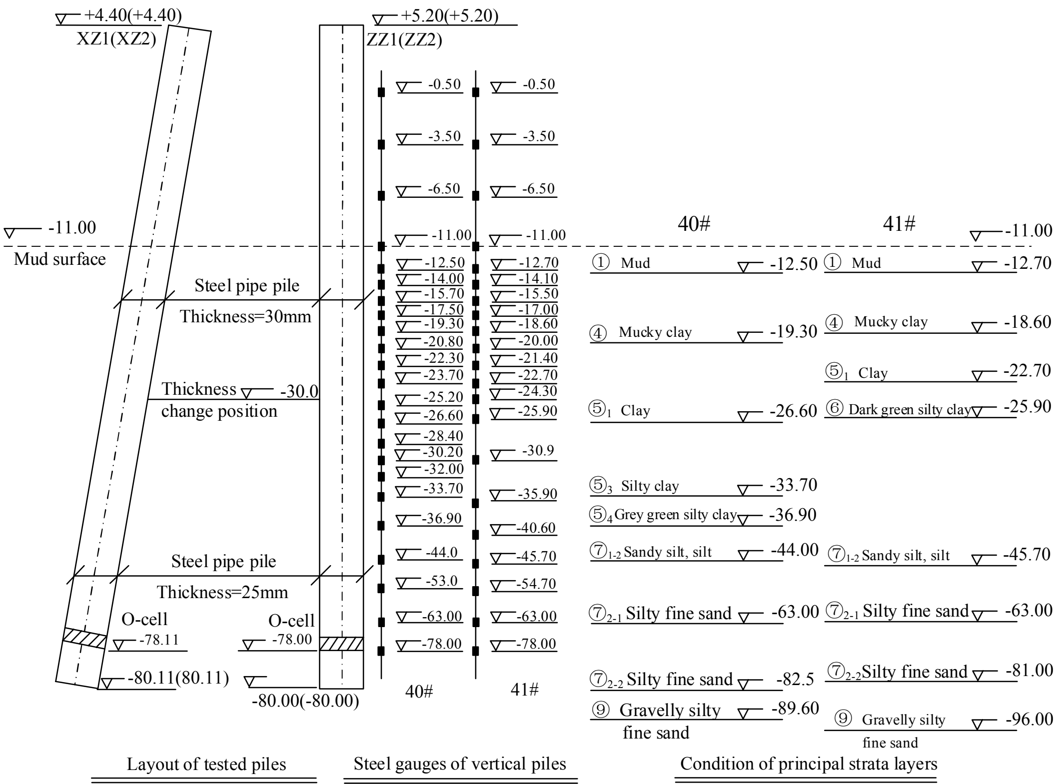

Figure 3: The evolution of the test pile, steel gauges, and soil layer

Table 2: Principal soil layers and parameters of soil

	Soil layer	ρ (g/cm^3)	w (%)	e	w_L (%)	w_P (%)	S_r (%)	c (kPa)	ϕ (°)
①	Mud	1.71	90.4	1.409	40.1	22.2	98	—	—
④	Mucky clay	1.65	90.4	1.618	45.9	25.3	98	5.8	2.3
⑤1	Clay	1.77	43.8	1.239	39.4	21.7	97	19.8	8.9
⑤3	Silty clay	1.95	30.2	0.834	37.8	20.9	95	35.8	11.3
⑤4	Grey green silty clay	1.97	29.8	0.732	38.6	21.3	95	21.0	22.9
⑥	Dark green silty clay	1.96	24.9	0.744	34.3	19.5	93	23.6	28.7
⑦1-2	Sandy silt, silt	1.93	27.4	0.706	30.8	—	96	3.8	32.8
⑦2-1	Silty fine sand	1.950	24.9	0.688	31.1	—	96	4.3	33.5
⑦2-2	Silty fine sand	1.98	25.3	0.659	29.5	—	97	4.7	33.3
⑨	Gravelly silty fine sand	2.08	15.7	0.497	27.5	5.4	88	5.2	34.5

3 METHODS

There were four piles conducted the axial bearing tests, and two piles were conducted the lateral bearing tests. The following are the methods of the axial test and the lateral test respectively. In order to minimize the effect of the bearing characteristic of inclined piles by waves, currents and tides (Ye and Zhou, 2004), the tests were carried out under calm sea condition.

3.1 THE AXIAL BEARING CAPACITY FIELD TESTS

The axial bearing capacity tests were conducted by O-cell test method. The O-cell test method is less susceptible to space limitations and can effectively achieve axial loading for the inclined pile compared with the static loading method and the anchor pile method. It involves embedment of a load cell near the pile base, and when the load cell is pressurized internally, the same upward and downward forces act on the pile shaft and pile base respectively at the same time. The distribution of the axial force of the pile can be established by testing the strain and stiffness of the pile section, and the frictional resistance in different layers also can be calculated. Thus, the tested *Q-s* curves of upward and downward could be converted into the equivalent *Q-s* curve of the top-loaded pile. The diagram of O-cell and measurement components installation are shown in Figure 4. There were six displacement sensors fixed on the reference beam by the magnetic base and measured the displacement of the tested pile. Two sensors were used to measure the upward displacement of O-cell cap, two were used to measure the downward displacement of O-cell bottom, and another two were used to measure the upward displacement of pile top. The slow load maintaining method was adopted in the tests, and the methods of loading and unloading followed the Chinese standard JT/T 738–2009 (The Traffic Professional Standards Compilation Group of People's Republic of China 2009). The normal load increments of every grade were 1400kN, and the first increment used twice the normal load rating and when the loading value was close to the designed maximum load, the load increments reduce to 700kN. The loading termination criteria were as follows: (*i*) The displacement was equal to 40 mm or more; in this loading grade, with a displacement of five times the last grade displacement or more, the previous loading is deemed to be the ultimate bearing capacity. (*ii*) The total displacement is 40 mm or more, and if the stable state is not reached within 24 hours under this loading level, the loading test can be terminated and the previous loading is regarded as the ultimate bearing capacity. (*iii*) If the total displacement is less than 40 mm, but the loading reaches the ultimate capacity of the load cell and or it exceeds the range of the load cell, loading can be terminated.

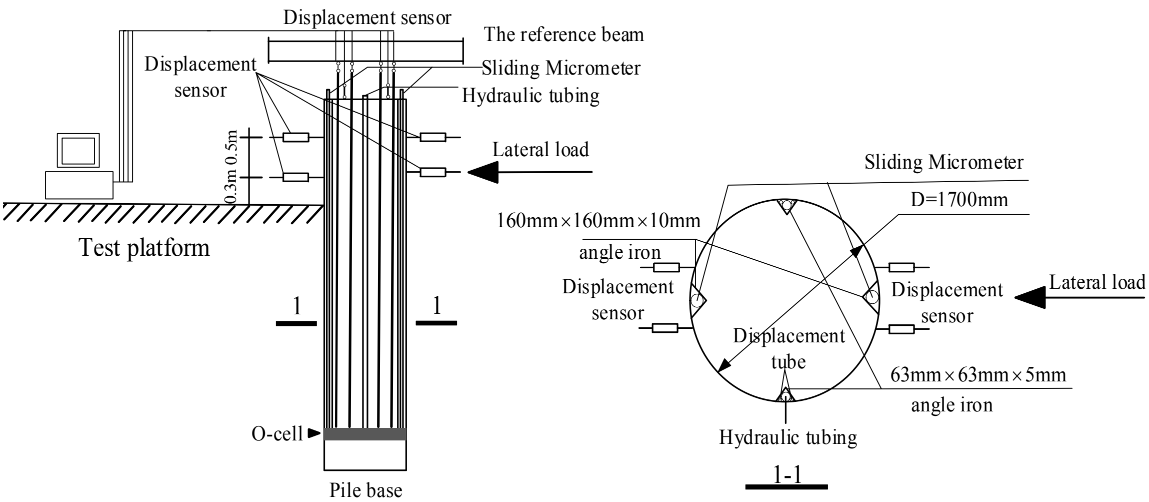

Figure 4: The O-cell and measurement components installation of field test

3.2 THE LATERAL BEARING CAPACITY TESTS

There were two piles (40#ZZ1and 41#ZZ2) conducted the lateral bearing capacity test. The lateral jack was disposed between the tested piles and other five piles, and the other five piles were connected as a whole to provide reaction force. Figure 5 shows the connecting method of the reaction pile and the testing pile through a ball joint, a jack, a load transfer rod, etc. The lateral one-way loop load maintaining method was adopted in the tests, and the methods of loading and unloading followed the Chinese standard JTS 167-4-2012. The loading value per step was one-twelfth of the maximum design lateral load, while the unloading value was twice that of the loading value. Each step of loading was maintained for 20 minutes, and each step of unloading was maintained for 10 minutes. The loading was terminated when the lateral deformation or the lateral deformation rate increased significantly, or if the lateral loading reached the maximum design value. There were eight displacement sensors fixed on the reference beam by the magnetic base to measure the lateral displacement of the tested pile. Two sensors measure the lateral displacement of the pile at the loading point, two sensors measure the lateral displacement of the pile at the back of loading point, two sensors measure the lateral displacement of 50cm above the plane of the lateral load, and other two sensors measure the lateral displacement of back of the pile of 50cm above the plane of lateral load. Pile bending moment was measured by sliding micrometre, and two slide tubes were symmetrically arranged on both sides of the pile. The displacement sensors and sliding micrometre tube installation are shown in Figure 4.

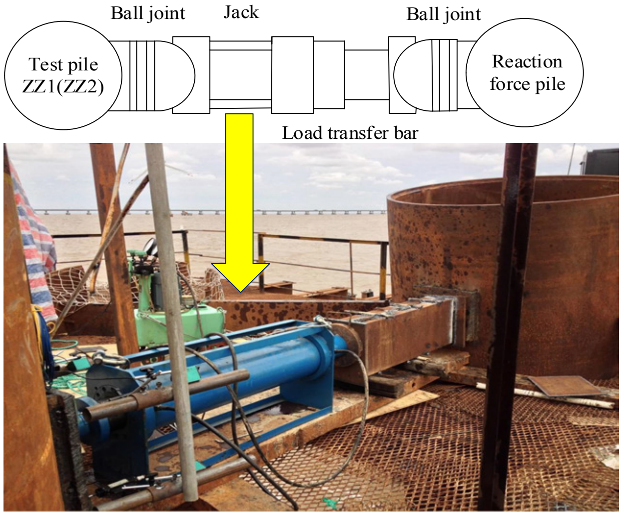

Figure 5: The Lateral field test

4 RESULTS

Based on the axial bearing capacity field test and lateral bearing capacity tests, the *Q-s* curves and *H-x* curves can be obtained, the test result as following, and the further discussion based on the test result are presented in the section of discussion.

4.1 THE *Q-S* CURVES OF AXIAL LOAD TEST

The test curves of 40#ZZ1, 40#XZ1, 41#ZZ2, and 41#XZ2 are shown in Figure 6(a)-(d). The lasting loading time of 40#ZZ1 pile was 10 hours and 21 minutes. As shown in Figure 6 (a), when it was loaded to the 9th grade (corresponding to the loading value of 2×12600kN), the downward displacement of the lower segment pile suddenly increased, and it rapidly increased to 90.46 mm, the upward displacement of the upper segment pile increased to 18.73 mm. Then, the bearing capacity of the lower segment pile reached the ultimate, and the loading was terminated.
The lasting loading time of 40#XZ1 pile was 9 hours and 22 minutes. See Figure 6 (b), when the pile was loaded to the 8th grade (corresponding to the loading value of 2×11200kN), the upward displacement of the upper segment pile suddenly increased and the displacement rapidly increased to 85.25 mm, the downward displacement of the lower segment pile increased to 24.38 mm, the bearing capacity of the upper segment pile reached the ultimate, and the loading was terminated.

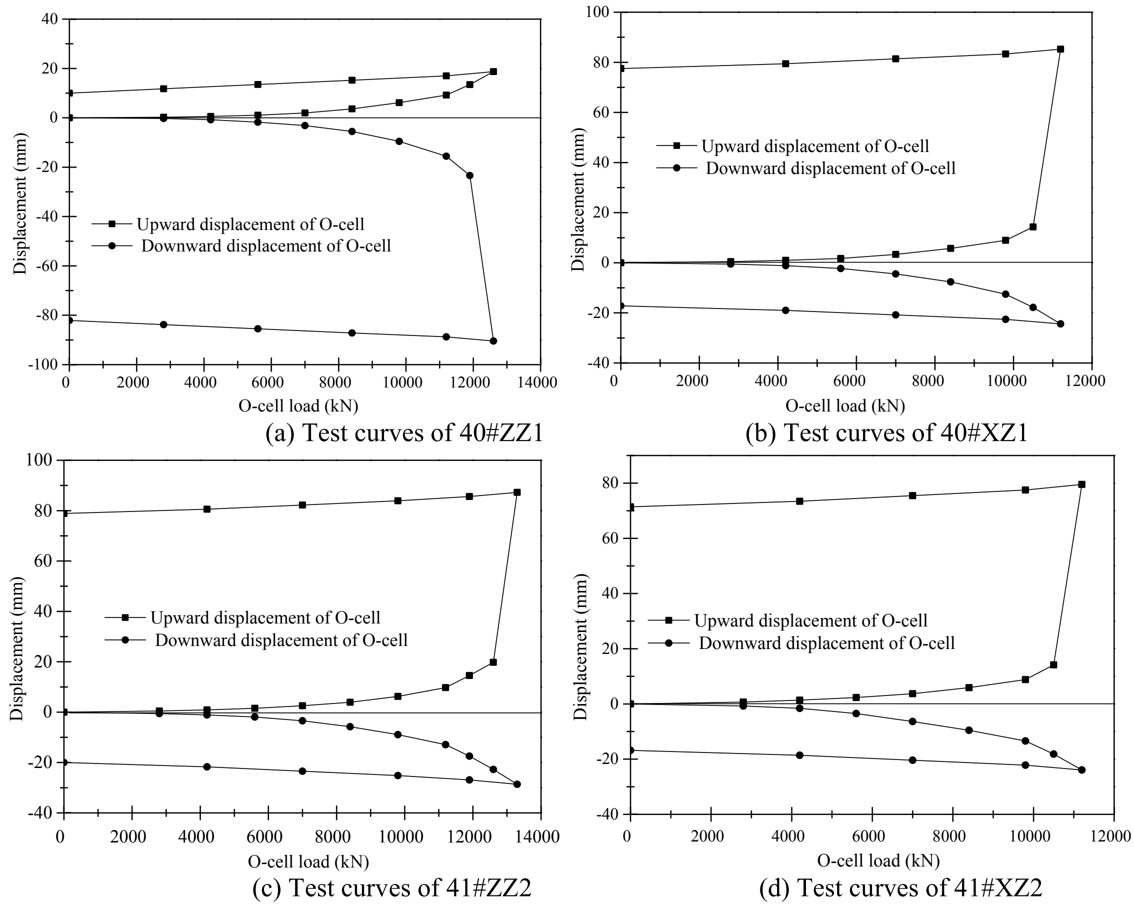

(a) Test curves of 40#ZZ1 (b) Test curves of 40#XZ1

(c) Test curves of 41#ZZ2 (d) Test curves of 41#XZ2

Figure 6: The *Q-s* curves of test pile

The lasting loading time of 41#ZZ2 pile was 11 hours and 24 minutes. As shown in Figure 6 (c), when it was loaded to the 10th grade (corresponding to the loading value of 2×13300kN), the upward displacement of the upper segment pile suddenly increased and the displacement rapidly increased to 87.26 mm, and the downward displacement of the lower segment pile increased to 28.63 mm, the bearing capacity of the upper segment pile reached the ultimate, and the loading was terminated.

The lasting loading time of 41#XZ2 pile was 9 hours and 28 minutes. As shown in Figure 6 (d), when it was loaded to the 8th grade (corresponding to the loading value of 2×11200kN), the upward displacement of the upper segment pile suddenly increased and the displacement rapidly increased to 79.53 mm, the downward displacement of the lower segment pile increased to 23.95 mm, the bearing capacity of the upper segment pile reached the ultimate, and the loading was terminated.

4.2 THE LOAD-DISPLACEMENT CURVES OF LATERAL LOAD TEST

During the test, the maximum design lateral load of the vertical pile was 480kN, and the increasing grade of loading was 40kN. The load-lateral displacement curves of the test piles（40#ZZ1 and 41#ZZ2）and the pile shaft deflection at each load increment are shown in Figure 7 and Figure 8.

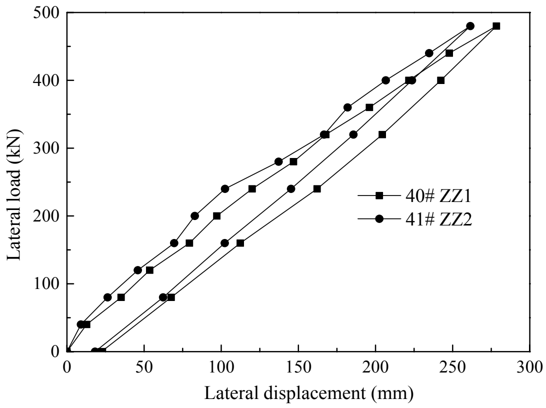

Figure 7: Load-displacement curves of 40#ZZ1 and 41#ZZ2

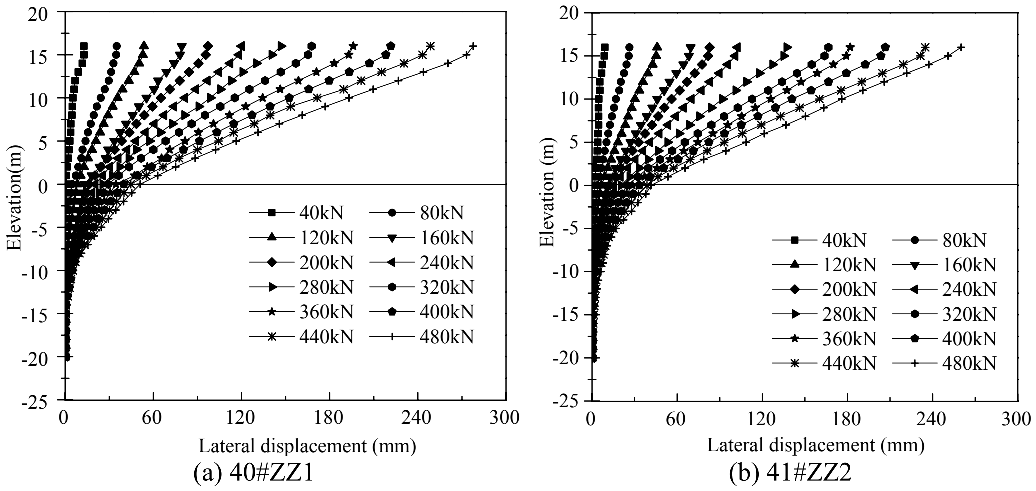

Figure 8: Pile shaft deflection at each load increment

It got from Figure 7 and Figure 8 that, the maximum displacement of the 40#ZZ1 pile head was 278.35mm when it was loaded to 480kN, and the displacement of pile shaft at mud surface was 51.05mm. The residual displacement of 40#ZZ1 was 22.38mm when it was unloaded to 0. The maximum displacement of the 41#ZZ2 pile head was 261.48mm when it was loaded to 480kN, and the displacement of pile shaft at mud surface was 46.69mm. The residual displacement of 40#ZZ2 was 18.22mm when it was unloaded to 0kN.

5 DISCUSSION

In this section, based on the axial test results and the measured strain values, the equivalent conversion results, the distributions of axial force and shaft resistance, and the relationship between the shaft resistance and relative displacement were all calculated and discussed. Moreover, based on the lateral test results and the measured strain values, the bending moment of pile shaft, the pile shaft deflection, and the *p*-*y* curves in different soil layers of 40#ZZ1 were all discussed as follows.

5.1 THE EQUIVALENT CONVERSION RESULTS

In the measurement of the pile bearing capacity with the O-cell test, the load generated by the load case, the axial displacement in two directions, and the strain of the pile at different layer depths can be determined. Based on the analytical method of load transfer, the relationship of the friction-deformation of the upper part of the pile and the load-deformation of the lower part of the pile can be converted into the traditional load-deformation manner in which the load acted on the pile top. This is called the equivalent top-loaded method, more details of conversion calculation method were discussed by Dai et al. (2010), and the equivalent curves are shown in Figure 9.

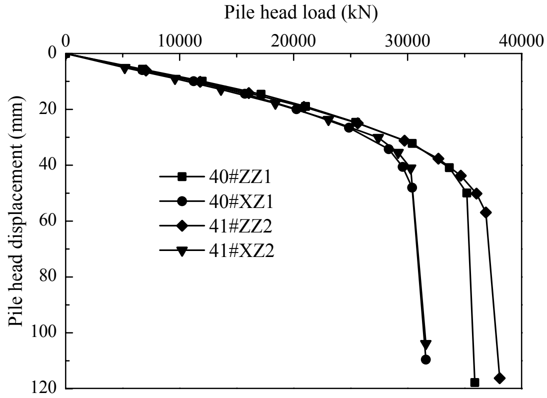

Figure 9: Equivalent *Q-s* curves of four test piles

The conversion results were calculated and plotted in Figure 9, it shows that the ultimate bearing capacity of the test piles (40#ZZ1, 40#XZ1, 41#ZZ2, and 41#XZ2) were 35196kN, 30399kN, 36863kN, and 30271kN, respectively. By Comparing the four curves in Figure 9, it can be seen that the basic trends of the bearing curves of the two vertical piles and the two inclined piles are similar, and the ultimate bearing capacity values are also close. The *Q-s* curve of inclined pile arrives earlier to the segment of slope changing than the *Q-s* curve of vertical piles, the axial ultimate bearing capacity of the two inclined piles is smaller than that of the vertical piles.

5.2 AXIAL FORCE DISTRIBUTIONS

Axial force distributions are very helpful in clarifying the mechanism of load transfer, and the test, the axial force of the pile changes with depth were calculted based on the strain gauges along the pile shaft. The axial force at can be obtained according to Equation (1).

$$F_i = \varepsilon E_s A_s \qquad (1)$$

where F_i is the axial force i (kN), ε is the strain at shaft section i, E_s, and A_s are the elastic modulus of the material of steel pipe pile and cross-sectional areas of pipe pile shaft (m[2]), respectively.

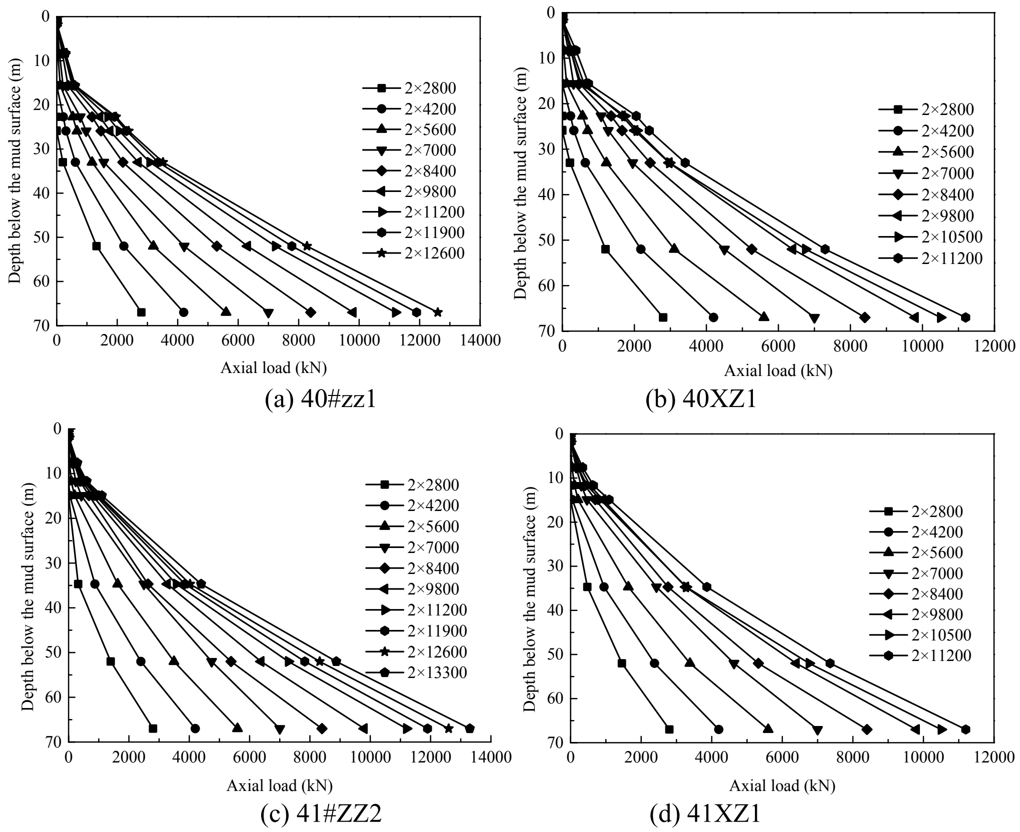

Figure 10: Axial force distributions of test pile at each load increment

The axial force distributions of the four test piles are shown in Figure 10 (a)-(d), it can be observed from the Figure 10 that axial force distributions of the shaft obtained by O-cell test method is different from that obtained by the top-down load test method. At each load increment, the distribution curve of the axial force of the shaft decreases gradually toward the top of the shaft, and there is no significant difference in the distributions of axial force for the two inclined piles and vertical piles.

5.3 SHAFT RESISTANCE

The values of the shaft resistance are affected by the relative displacement between the piles and soils, the stiffness ratio of the piles and soils, and the lateral force on the pile shaft and soil properties. Based on the axial force of the shaft and the parameters of the shaft section, the shaft resistance of the different soil layers is determined by Equation (2).

$$\tau_i = \frac{\Delta F}{A} = \frac{F_{i+1} - F_i}{\pi D h_i} \qquad (2)$$

where, τ_i is the side resistance at section i (kPa), ΔF is the variation of the axial force between the section F_{i+1} and F_i, A is the area surrounding the pile between the section F_{i+1} and F_i, D is the shaft diameter (m), and h_i is the length of the shaft in soil between the section F_{i+1} and F_i (m).

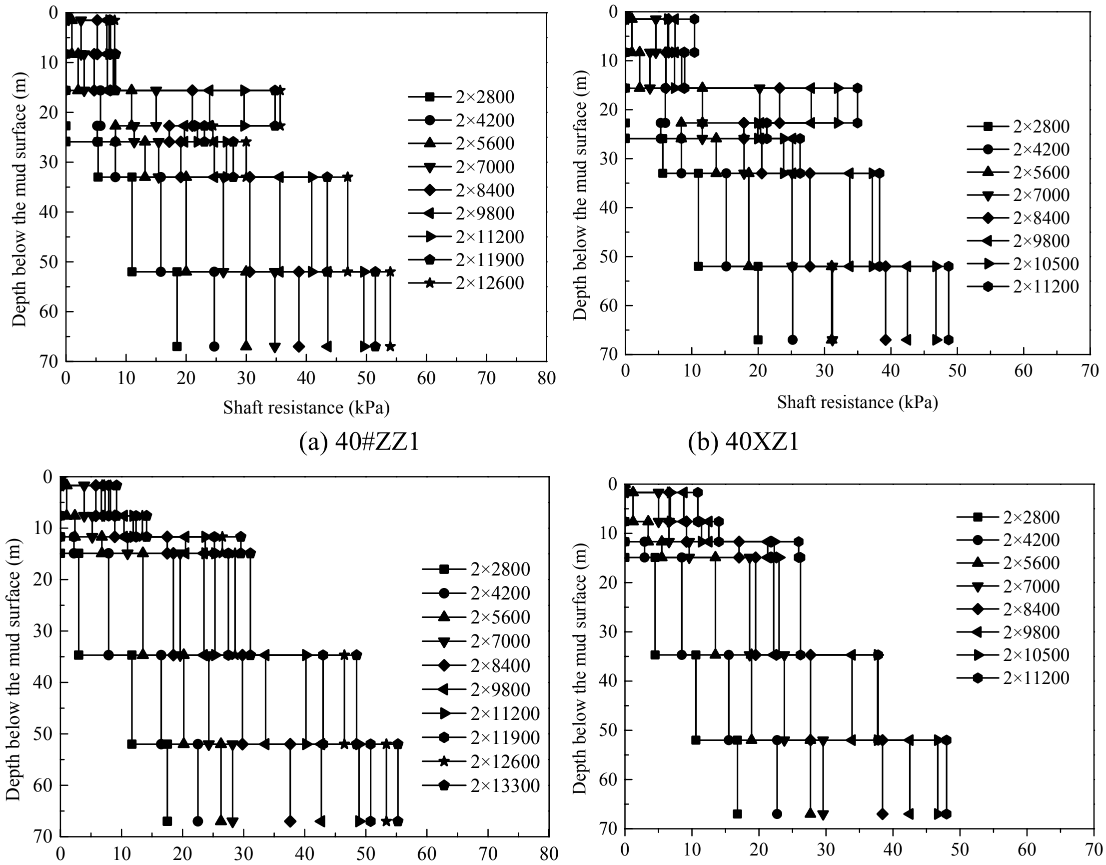

Figure 11: Shaft resistance distributions of test pile at each load increment

It can be seen from Figure 11 (a)-(d) that during the test, as the applied load increases, the shaft resistance was gradually mobilized and increased. Under each load increment, the mobilized shaft resistance of the test shafts in the soil layers adjacent to the load cell is the largest, and as away from the load cell, the mobilized shaft resistance was gradually reduced, and at the mud surface, the mobilized shaft resistance decreased to zero. Comparing Figure 11 (a) and (b), (c) and (d) respectively, it can be seen that when the load cell was loaded to the maximum load, the mobilized shaft resistance at different depths of the two vertical piles larger than two inclined piles. Moreover, at the site of foundation #40, the soil layer ⑤$_3$ (silty clay) show a relatively strong potential shaft resistance due to the curve shape presented, at the site of foundation #41, the soil layer ⑥ (dark green silty clay) has a relatively strong shaft resistance.

5.4 THE RELATIONSHIP BETWEEN SHAFT RESISTANCE AND RELATIVE DISPLACEMENT OF PILE-SOIL

The relative displacement between the pile shaft and soil is an important factor affecting the shaft resistance that will eventually affect the ultimate bearing capacity and displacement of the shaft, which is accepted as common sense among researchers. Unfortunately, it is rather difficult to determine the actual displacements between the piles shaft and soils. Therefore, it is assumed that the soil displacement is not moving during static load tests and not affected by the shaft displacement in this study. That is, the relative displacement between the shaft and soil at a specified depth is equal to the shaft displacement at the same depth, and its values in different soil layers can be obtained by Equation (3).

$$S_i = S_t - \sum_{i=1}^{i} L_i(\varepsilon_i + \varepsilon_{i+1})/2 \qquad (3)$$

Where S_i is relative displacement between the soil layer *i* and the pile shaft, *St* is the upward or downward displacement of the O-cell, L_i is the thickness of the soil layer *i*, and ε_i *and* ε_{i+1} are the strains of the pile shaft at the top and bottom section of the soil layer *i,* respectively. By using the strain data, the relation between the relative displacement of pile-soil and shaft resistance of pile for different soil layers is illustrated in Figure 12.

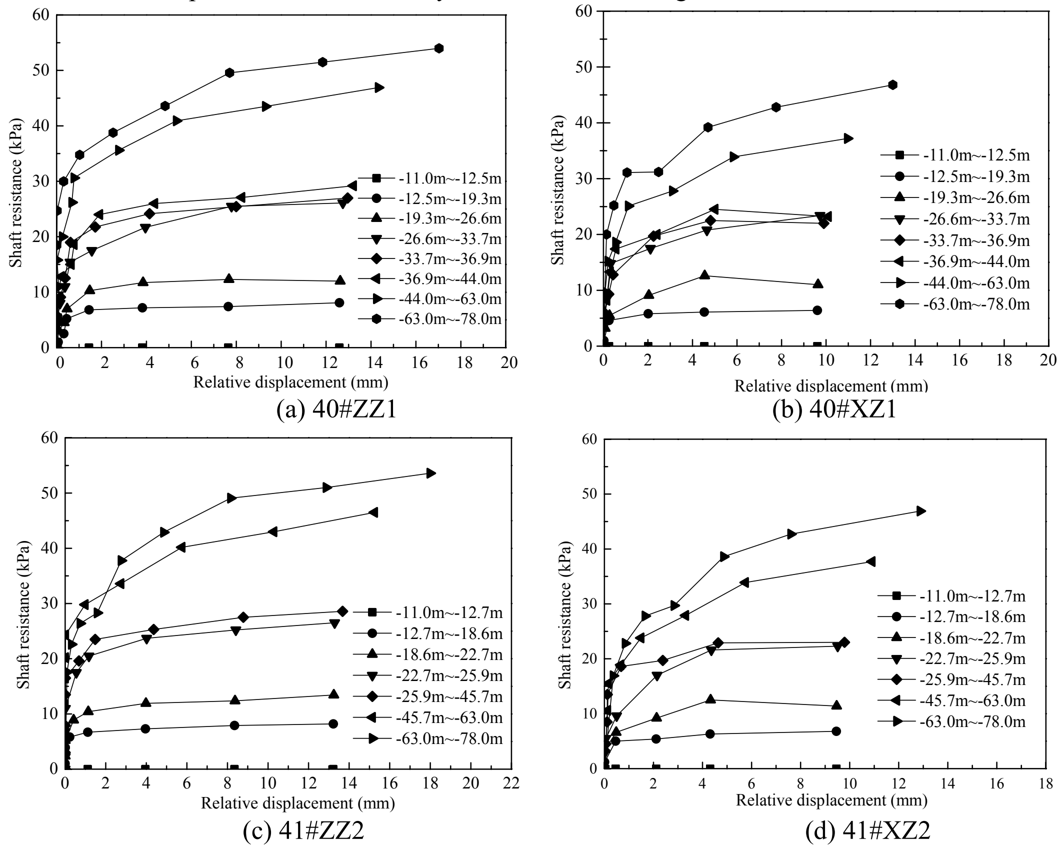

Figure 12: Relationship between the shaft resistance and relative displacement of pile-soil

From the curves of shaft resistance and pile-soil relative displacement in Figure 12 (a)-(d), it can be seen that the shaft resistance within the range of -1.0-12.7m below the seabed surface is almost zero, and the limit value of shaft resistance increases with the depth increases. As the relative displacement of pile and soil gradually increase, the shaft resistance increases nonlinearly which contained the linear increase phase, the yielding phase, and finally reach the limit value. It can be seen from Figure 12 (a) that as the depth increases, the limit value of the shaft resistance of 40#ZZ1test pile increases gradually. The limit values of the shaft resistance in the range of -12.5m~-78.0m are 8.09kPa, 11.99kPa, 26.10kPa, 26.99kPa, 29.19kPa, 46.90kPa, 53.99kPa, respectively. Figure 12 (b) shows that as the depth increases, the limit value of the shaft resistance of 40#XZ1test pile increases gradually. The limit values of the shaft resistance in the range of -12.5m~-78.0m are 6.40kPa, 11.02kPa, 23.40kPa, 22.5kPa, 24.5kPa, 37.2kPa, 46.8kPa, respectively. Figure 12 (c) shows that as the depth increases, the limit value of the shaft resistance of 41#ZZ2test pile increases gradually. The limit values of the shaft resistance in the range of -12.7m~-78.0m are 8.18kPa, 13.42kPa, 26.50kPa, 28.58kPa, 46.50Pa, 53.95kPa, respectively. Figure 12 (d) shows that as the depth increases, the limit value of the shaft resistance of 41#XZ2 test pile increases gradually. The limit values of the shaft resistance in the range of -12.7m~-78.0m are 6.80kPa, 11.42kPa, 22.34kPa, 23.02kPa, 37.71Pa, 46.90kPa, respectively. By compared the above data, at the same depth, the shaft resistance limit value of the 40#ZZ1 was larger than that of 40#XZ1, and the shaft resistance limit value of 41#ZZ2 was also larger than 41#XZ2.

5.5 THE BENDING MOMENT OF PILE SHAFT

According to the results of strain value, the pile bending moment was calculatedd. The results are shown as Figure 13. As it shows, the maximum bending moment of 40#ZZ1 pile was 10321.86kNm, and the maximum bending moment of 41# ZZ2 pile was 9732.67kNm. As the lateral load increases, the maximum section of the bending moment is gradually moved down from 4.5m to 7.5m under the mud surface, which was located below the mud surface at a depth of 2.6-4.4 times of the pile diameter.

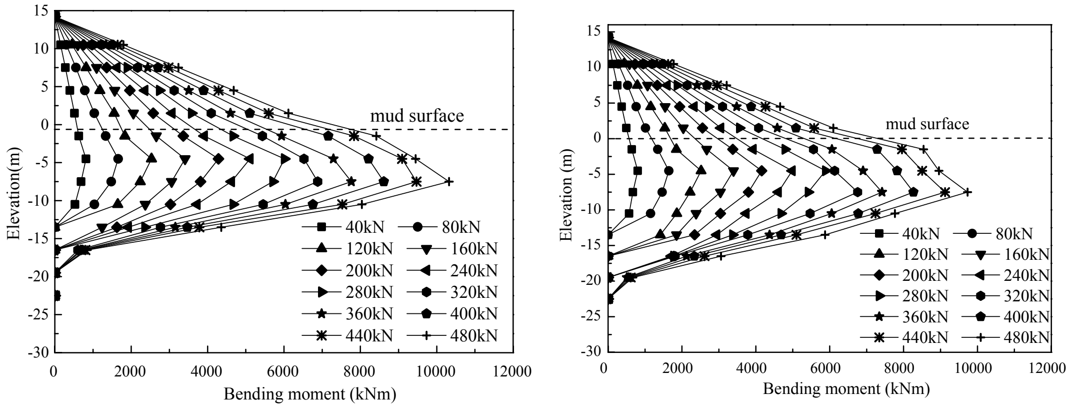

(a) 40#ZZ1 (b) 41#ZZ2

Figure 13: Pile bending moment at each load increment

5.6 THE PILE SHAFT DEFLECTION

The bending deflection of the shaft axis was calculated directly by the bending strain which was tested by strain gauges at different sections in the tests (shown in Figure 3). In the test, the strain gauges were arranged in pairs for all every section, which was essentially a fixed miniature inclinometer. The calculation precision of deflection curve of the pile by the bending strain was high, and calculation model is shown in Figure 14. Since the parameters of 40#ZZ1 test pile almost same as 41#ZZ2, and the test results are basically the same, thus, take 40#ZZ1 as an example for analysis.

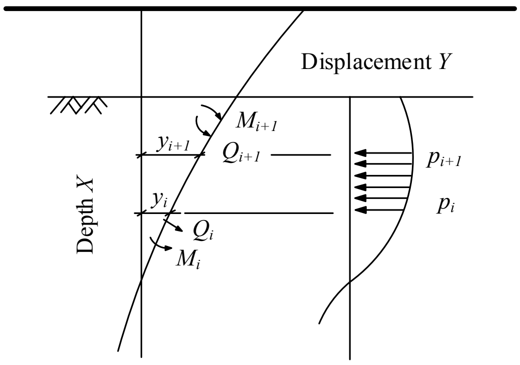

Figure 14: Calculation model of pile shaft deflection

The bending strain distribution of the adjacent section was assumed as a straight line, the strain at the distance of x to node i in different segments is as follows:

$$\Delta\varepsilon=\Delta\varepsilon_i+(\Delta\varepsilon_{i+1}-\Delta\varepsilon_i)x/l_i \qquad (4)$$

Given by mechanics of materials:

$$EI\frac{d^2y}{dx^2}=-\frac{EI(\varepsilon_+-\varepsilon_-)}{b_0} \qquad (5)$$

Substituting Equation (4) to Equation (5), Equation (6) can be obtained as:

$$\frac{d^2y}{dx^2}=-\frac{[\Delta\varepsilon_i+(\Delta\varepsilon_{i+1}-\Delta\varepsilon_i)x/l_i]}{b_0} \qquad (6)$$

The rotation and displacement at all section of the pile shaft can be obtained by integrating Equation (6) once and twice

$$\theta_{i+1} = \theta_i - (\Delta\varepsilon_{i+1} + \Delta\varepsilon_i)\frac{l_i}{2b_0} \quad (7)$$

$$y_{i+1} = y_i + \theta_i l_i - (\Delta\varepsilon_{i+1} + 2\varepsilon_i)\frac{l_i^2}{6b_0} \quad (8)$$

Where, EI is the bending stiffness of the pile, b_0 is the distance of two tested sections; $\triangle\varepsilon_i$ and $\triangle\varepsilon_{i+1}$ is the bending strain of section i and i+1 respectively; θ_i and θ_{i+1} is the rotation of section i and i+1 respectively; y_i and y_{i+1} is the lateral displacement of section i and i+1 respectively; l_i is the length of unit i. The pile shaft deflection along the depth calculated by using the above Equations (4-8), and the results is shown in Figure 15.

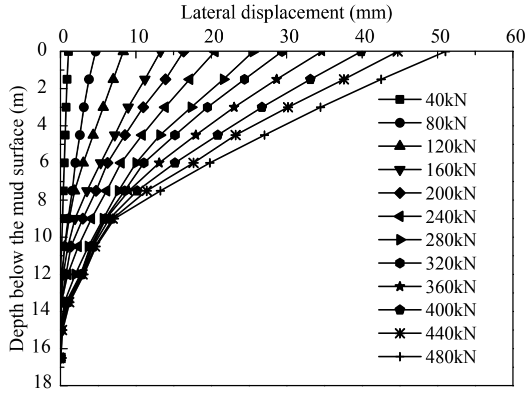

Figure 15: The deflection of the pile shaft with the load of 40kN and 480kN

From Figure 15, it can be seen that as the load increased from 40kN to 480kN, the deflection of the pile shaft at the mud surface and the depth of the section where the pile shaft is deflected increased and the deflection of the pile also gradually changed from linear to nonlinear. The deflection of the pile shaft under the mud surface of 16.5 m could be ignored.

5.7 THE *p-y* CURVES IN DIFFERENT SOIL LAYERS OF 40#ZZ1

The soil resistance at the side of the pile was obtained by differentiating the shearing force once and dividing it by the pile width. Then, by using the results of soil resistance and the deflection of the pile shaft, the *p-y* curves in different soil layers of 40#ZZ1 is plotted in Figure 16.

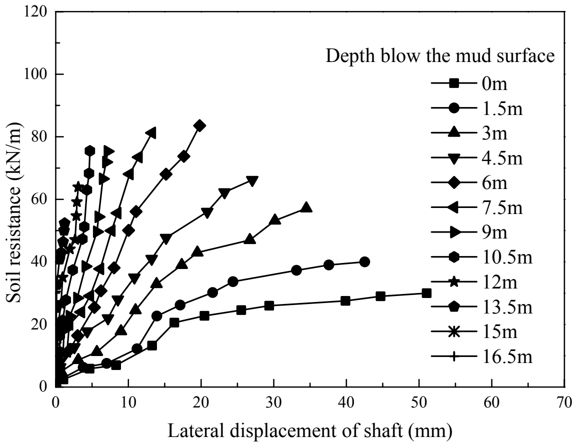

Figure 16: p-y curves in different soil layers of 40#ZZ1

It can be seen from Figure 16 that, as the lateral displacement of the pile shaft gradually increases, soil resistance at also gradually increases overall. Observing the curves in Figure 16, it can be seen that the soil resistance at the mud surface gradually yields with the increase of the displacement of and reaches the limit value, and the curve shape is hyperbolic. The limit value of the soil resistance at mud surface was 30.21kN/m. As the depth increases, the slope of the soil resistance curve gradually increases. The soil resistance curve within 6m below the mud surface shows a significant nonlinear relationship, while the soil resistance curves in the range of -6m~-16.5m is still in the linear stage.

6 CONCLUSIONS

Conclusions can be drawn according to the above results and discussion:

The equivalent conversion results showed that the ultimate bearing capacity of the four test pile (40#ZZ1, 40#XZ1, 41#ZZ2, and 41#XZ2) was 35196kN, 30399kN, 36863kN, and 30271kN, respectively. The axial ultimate bearing capacity of the inclined pile (the inclination is 12°) is significantly smaller than that of the vertical pile.

The maximum lateral displacement of the pile head of 40#ZZ1 and 41#ZZ2 was 278.35mm and 261.48mm respectively when loaded to 480kN, and the displacement of pile shaft at mud surface was 51.05mm and 46.69mm. The residual displacement of the pile head of 40#ZZ1 and 41#ZZ2 was 22.38mm and 18.22mm when it was unloaded to 0kN.

The mobilized shaft resistance at different depths of the two vertical piles was larger than two inclined piles when loaded to the maximum load. Moreover, the soil layer ⑤$_3$ (silty clay) and ⑥ (dark green silty clay) show a relatively strong potential shaft resistance.

As the relative displacement of pile and soil gradually increase, the shaft resistance increases nonlinearly which contained the linear increase phase, the yielding phase, and finally reach the limit value. And, at the same depth, the shaft resistance limit value of the 40#ZZ1 was larger than that of 40#XZ1, and the shaft resistance limit value of 41#ZZ2 was also larger than 41#XZ2.

As the lateral displacement of the pile shaft gradually increases, the soil resistance at the mud surface gradually yields with the increase of the displacement of and reaches the limit value, and the curve shape is hyperbolic. The limit value of the soil resistance at mud surface was 30.21kN/m, and the soil resistance curve within 6m below the mud surface shows a significant nonlinear relationship, while the soil resistance curves in the range of -6m~-16.5m is still in the linear stage.

CONFLICTS OF INTEREST

The authors declare that there are no conflicts of interest regarding the publication of this paper.

ACKNOWLEDGEMENTS

This study is supported by Natural Science Foundation of Jiangsu Province (BK20230599), China Postdoctoral Science Foundation (2023M742959), The Natural Science Foundation of the Jiangsu Higher Education Institutions of China (22KJB560034), The Innovation and Entrepreneurship Program of Jiangsu Province (JSSCBS20211051).

CRediT authorship contribution statement

Jiang Xu: Conceptualisation, Writing – original draft, Funding acquisition. **Yuhe Xia:** Investigation. **Weiming Gong:** Investigation, Supervision. **Huifang Deng:** Validation. **Zhengwei Bai:** Visualization. **Yuanbing Chen:** Resources.

REFERENCES

IEA (International Energy Agency), 2007. Renewables in global energy supply: An IEA fact sheet. Paris: OECD/IEA, 34p.

Alari, Victor, and Urmas Raudsepp. 2012. Simulation of wave damping near coast due to offshore wind farms, *Journal of Coastal Research*, 28: 143-48.

Dai, Guoliang, Weiming Gong, Xueliang Zhao, and Xiangqin Zhou. 2010. Static testing of pile-base post-grouting piles of the Suramadu bridge, *Geotechnical Testing Journal*, 34: 34-49.

De Nicola, Antony, and MF Randolph. 1997. The plugging behaviour of driven and jacked piles in sand, *Geotechnique*, 47: 841-56.

Fan, Chia-Cheng, and James H Long. 2005. Assessment of existing methods for predicting soil response of laterally loaded piles in sand, *Computers and Geotechnics*, 32: 274-89.

Feng, S-j, H Ke, Y-m Chen, J-g Zheng, and B-x Ru. 2004. Experimental study on super-long bored pile in loess, *Chinese Journal of Geotechnical Engineering-Chinese edition-*, 26: 110-14.

Feng, Shi-Jin, Shi-Feng Lu, and Zhen-Ming Shi. 2016. Field investigations of two super-long steel pipe piles in offshore areas, *Marine Georesources & Geotechnology*, 34: 559-70.

Gao, Rui, Youjin Zeng, and Bin Zhu. 2011. Centrifuge model testing on super-long rock-socketed bored piles under vertical loading, *Geomechanics and Geoengineering: An International Journal*, 6: 21-29.

Haiderali, Aliasger, and Gopal Madabhushi. 2012. Three-dimensional finite element modelling of monopiles for offshore wind turbines. In *Proceedings of the world congress on advances in civil, environmental, and materials research, Seoul*, 3277-95.

Jardine, RJ. 1996. New design methods for offshore piles, *Publication MTD 96/103*.

Lehane, BM, and KG Gavin. 2001. Base resistance of jacked pipe piles in sand, *Journal of Geotechnical and Geoenvironmental Engineering*, 127: 473-80.

Lesny, K, and J Wiemann. 2006. Finite-element-modelling of large diameter monopiles for offshore wind energy converters. in, *GeoCongress 2006: Geotechnical Engineering in the Information Technology Age*.

Li, Shu-cai, Qian Zhang, Qian-qing Zhang, and Li-ping Li. 2016. Field and theoretical study of the response of super-long bored pile subjected to compressive load, *Marine Georesources & Geotechnology*, 34: 71-78.

Liu, Run, Long Zhou, Ji-jian Lian, and Hong-yan Ding. 2015. Behavior of monopile foundations for offshore wind farms in sand, *Journal of Waterway, Port, Coastal, and Ocean Engineering*, 142: 04015010.

Nicola, A DE, and MF Randolph. 1999. Centrifuge modelling of pipe piles in sand under axial loads, *Geotechnique*, 49: 295-318.

Paik, Kyuho, and Rodrigo Salgado. 2003. Determination of bearing capacity of open-ended piles in sand, *Journal of Geotechnical and Geoenvironmental Engineering*, 129: 46-57.

Paikowsky, Samuel G, and Robert V Whitman. 1990. The effects of plugging on pile performance and design, *Canadian Geotechnical Journal*, 27: 429-40.

Snyder, Brian, and Mark J Kaiser. 2009. Ecological and economic cost-benefit analysis of offshore wind energy, *Renewable Energy*, 34: 1567-78.

Wang, WD, YH Li, and JB Wu. 2011. Field loading tests on large-diameter and super-long bored piles of Shanghai Center Tower, *Chinese Journal of Geotechnical Engineering*, 33: 1817-26.

Wang, ZF, HD Liu, JL Jia, ZQ Huang, and Tong Jiang. 2012. Experimental study of vertical bearing capacity behavior of large-diameter bored cast-in-situ long pile, *Rock and Soil Mechanics*, 33: 2663-70.

Yu, Feng, and Jun Yang. 2011. Base capacity of open-ended steel pipe piles in sand, *Journal of Geotechnical and Geoenvironmental Engineering*, 138: 1116-28.

Zou, Xin-jun, and Ming-hua Zhao. 2013. Axial bearing behavior of super-long piles in deep soft clay over stiff layers, *Journal of Central South University*, 20: 2008-16.